

A numerical study of planar discharge motion

F. Benkhaldoun^a, J. Fořt^b, K. Hassouni^c, J. Karel^{a,b}, D. Trdlička^{b,*}

^aLAGA, University Paris 13, 99 Av. J. B. Clement, 93430 Villetaneuse, France

^bFaculty of Mechanical Engineering, CTU in Prague, Karlovo namesti 13, 121 35 Prague, Czech Republic

^cLSPM, University Paris 13, 99 Av. J. B. Clement, 93430 Villetaneuse, France

Received 28 March 2014; received in revised form 27 June 2014

Abstract

Presented paper describes a numerical study of discharge plasma motion. This non-stationary phenomenon with steep gradients and sharp peaks in unknowns is described as a coupled problem of convection-diffusion equation with source term for electron, ion densities and Poisson's equation for electric potential. The numerical method is 2nd order of accuracy in space and time and it uses dynamical adaptation of unstructured triangular mesh. Results of numerical studies included size of computational domain, type of boundary conditions and numerical convergence test are presented.

© 2014 University of West Bohemia. All rights reserved.

Keywords: numerical study, cold plasma, refinement, boundary conditions

1. Introduction

We deal with a numerical simulation of planar discharge motion. This phenomenon is also denoted as cold plasma motion, or avalanche of electrons or in 3D version as, e.g., streamer. The streamer motion simulation is subject of many scientific works, which consider either axisymmetric or fully 3D configuration, e.g., [1–5, 7]. Nevertheless, there is still a lot of challenging problems like, e.g., simulation of streamer in complicated geometries, streamer branching. This phenomenon can be used in different technical applications. In our case, we simulated the 2D discharge between two planar electrodes initializing by a narrow Gaussian pulse of charged particles of seven orders magnitude. The developed method will be next also extended into 3D.

2. Governing equations

We consider the so called minimal plasma model (see, e.g., [5] and [7]), which consists of two transport equations for electron and ion densities (\mathbf{n}_e , \mathbf{n}_i) coupled with Poisson's equation for the electric field potential V

$$\frac{\partial \mathbf{n}_e}{\partial t} + \operatorname{div}(\mathbf{n}_e \vec{v}_e - D_e \vec{\nabla} \mathbf{n}_e) = S_e, \quad (1)$$

$$\frac{\partial \mathbf{n}_i}{\partial t} = S_i^+, \quad (2)$$

$$\Delta V = -\frac{e(\mathbf{n}_i - \mathbf{n}_e)}{\epsilon \cdot 10^4}, \quad (3)$$

*Corresponding author. Tel.: +420 224 357 439, e-mail: david.trdlicka@fs.cvut.cz.

where \vec{v}_e is the electron drift velocity, S_e is the electron source term, the positive ion source term is simplified as $S_i^+ = S_e$, the diffusive coefficient D_e , the unit electron charge e , the dielectric constant ϵ and the intensity of electric field is computed by $\vec{E} = -\vec{\nabla}V$.

The source term and diffusive coefficient are computed by the following formulas (see, e.g., [6]):

$$S_e = \frac{\alpha}{N} \cdot \|\vec{v}_e\| \cdot \mathbf{n}_e, \quad (4)$$

$$\text{if } \frac{\|\vec{E}\|}{N} > 1.5 \cdot 10^{-15} \quad \frac{\alpha}{N} = 2 \cdot 10^{-16} \cdot \exp\left(\frac{-7.248 \cdot 10^{-15}}{\|\vec{E}\|/N}\right), \quad (5)$$

$$\text{else} \quad \frac{\alpha}{N} = 6.619 \cdot 10^{-17} \cdot \exp\left(\frac{-5.593 \cdot 10^{-15}}{\|\vec{E}\|/N}\right), \quad (6)$$

$$D_e = \left[0.3341 \cdot 10^9 \cdot \left(\frac{\|\vec{E}\|}{N}\right)^{0.54069} \right] \cdot \frac{\|\vec{v}_e\|}{\|\vec{E}\|}, \quad (7)$$

$$N = 2.5 \cdot 10^{19} \text{ cm}^{-3}, \quad (8)$$

where α is the ionization coefficient and N is the neutral gas density.

3. Numerical method

The sufficiently accurate computation inside moving narrow region of discharge head (characterized by very steep gradients of unknowns) is the crucial point of numerical simulation. Therefore, our numerical method is based on the unstructured dynamically adapted grid. We use the following algorithm for computation of unknowns in the new time (t^{k+1}) level:

1. Computation of \mathbf{n}_e^{k+1} , \mathbf{n}_i^{k+1} from evolution equations (1), (2).
2. Computation of V with results of step 1 on the right hand side of Poisson's equation (3).
3. Computation of \vec{E} , \vec{v}_e , D_e and S_e from equations (4)–(8).

We approximate the equation for the electron density (1) by the finite volume method. It leads to

$$\mathbf{n}_{e_i}^{k+1} = \mathbf{n}_{e_i}^k - \frac{\Delta t}{\mu_i} \text{Rez}_{e_i}^k, \quad (9)$$

$$\text{Rez}_{e_i}^k = \sum_{j=1}^m (\mathbf{n}_{e_{ij}}^k \vec{v}_{e_{ij}} n_{ij}^{\vec{v}} ds_{ij} - D_{e_{ij}} ((\mathbf{n}_{e_{ij}})_x, (\mathbf{n}_{e_{ij}})_y) n_{ij}^{\vec{v}} ds_{ij}) + S_{e_i}, \quad (10)$$

where Δt is a time step, m is the number of faces of the cell i , \vec{n}_{ij} is a unit normal vector of the face ij (between volumes i and j) and ds_{ij} is its length. Other variables denoted by the subscripts ij represent variables on the face ij . The convective flux is computed by the upwind scheme

$$\begin{aligned} \mathbf{n}_{e_{ij}} &= \mathbf{n}_{e_i} \quad \text{if } (\vec{v}_{e_{ij}} \cdot \vec{n}_{ij}) \geq 0, \\ \mathbf{n}_{e_{ij}} &= \mathbf{n}_{e_j} \quad \text{in other case,} \end{aligned} \quad (11)$$

the normal vector \vec{n}_{ij} is oriented from the cell i to the cell j . The gradient components $(\mathbf{n}_{e_{ij}})_x$, $(\mathbf{n}_{e_{ij}})_y$ in the center of edge (face) ij are computed on a dual cell with a central diamond scheme. Unknowns in the vertices of the edge are computed by the least square method.

Discretization of the equation for the ion density is based also on a forward difference for the time derivative

$$\mathbf{n}_i^{n+1} = \mathbf{n}_i^n + \Delta t S_i^+ \quad (12)$$

The Poisson's equation for the electric potential is discretized by a central finite volume approximation. We use a similar finite volume approximation as for diffusive terms in the equation for electron density. It leads to a system of linear equations

$$A\vec{V}^{n+1} = \vec{b}^{n+1}, \quad (13)$$

where A is a matrix of coefficients, \vec{V} is a vector of unknowns and \vec{b} is a vector of the right hand side. An i -th row in the matrix A corresponds to the cell i .

The system of equations (13) is solved directly by LU decomposition in an implementation for sparse matrices (with Intel MKL library). Numerical scheme used for evolution equation is first order of accuracy in time (explicit Euler's scheme) and space (approximation of convective term). The scheme for the Poisson's equation is second order of accuracy. Next the scheme for evolution equations has been extended into the theoretically second order of accuracy. The three stage Runge-Kutta scheme has been used for approximation in time

$$\begin{aligned} \mathbf{n}_e^{(0)} &= \mathbf{n}_e^{(k)}, \\ \mathbf{n}_e^{(1)} &= \mathbf{n}_e^{(0)} - \frac{1}{2}\Delta t \text{Rez}_e^{(0)}, \\ \mathbf{n}_e^{(2)} &= \mathbf{n}_e^{(0)} - \frac{1}{2}\Delta t \text{Rez}_e^{(1)}, \\ \mathbf{n}_e^{(k+1)} &= \mathbf{n}_e^{(2)} \end{aligned} \quad (14)$$

and second order approximation of convective term in (10) has been achieved by linear reconstruction and Barth-Jespersion limiter.

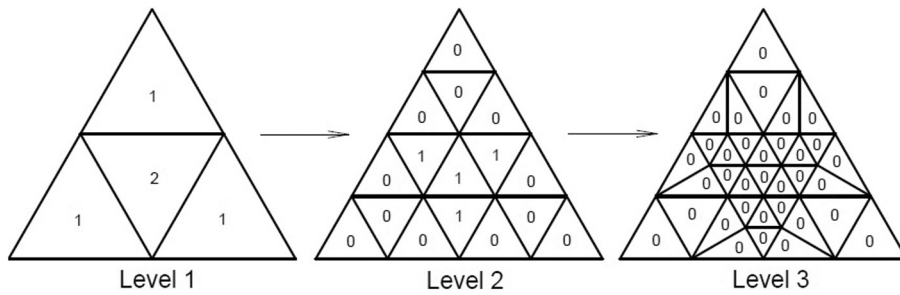


Fig. 1. Mechanism of multi-level mesh refinement

The dynamic mesh adaptation is used to capture sharp peaks and steep gradients of unknowns. The triangle of (starting) reference grid can be divided to 4^r triangles according to a refinement criterion (where r is the refinement level), see Fig. 1. The criterion is considered as a grid function, which has some non-zero value in each triangle of reference grid. These values are firstly smoothed by computation of several time steps of the simple diffusion equation. This is approximated by the explicit scheme and criterion function is used as the initial condition.

The values are then scaled into interval $\langle 0, 1 \rangle$. The interval $\langle 0, 1 \rangle$ is split into sub-intervals with prescribed level of adaptation. When the level of adaptation is evaluated for each triangle, the grid conformity procedure is applied. The new adapted grid is then generated and values of unknowns are conservatively interpolated from the previous adapted grid into the new one. The adapted grid is fixed for a prescribed number of time steps and then the grid adaptation procedure is repeated. The criterion consists of two parameters: the electron density gradient and the source term magnitude.

4. Problem formulation

We simulated planar discharge motion in homogenous electric field described by equations (1)–(7). This field is generated in a gaseous gap between two planar electrodes with high electric potential. We simulated this phenomenon in rectangular domain $x \times y = \langle 0; 1 \rangle \times \langle 0; 0.5 \rangle$ [cm] (standard calculation). Left ($x = 0$ cm) and right ($x = 1$ cm) boundaries are the plane anode and cathode, respectively. Upper ($y = 0.5$ cm) and lower ($y = 0$ cm) boundaries are artificial. They made the computational domain finite and sufficiently small.

We used the common initial distribution of charged particles for considered shape of electrodes, which represents a small electrically neutral region with high density of particles and proper background density of particles, which substitute neglected effect of photo-ionization. The corresponding electric potential in initial time is a linear function of the x coordinate

$$\begin{aligned} \mathbf{n}_e(x, y, 0) &= 10^{16} \exp\left(\frac{-(x - x_0)^2 + (y - y_0)^2}{0.01^2}\right) + 10^9 \text{ [cm}^{-3}\text{]}, \\ \mathbf{n}_i(x, y, 0) &= \mathbf{n}_e(x, y, 0) \text{ [cm}^{-3}\text{]}, \\ V(x, y, 0) &= 25\,000(1 - x) \text{ [V]}. \end{aligned} \quad (15)$$

Initial Gaussian pulse is placed in $[x_0; y_0] = [0.2; 0.25]$ cm. Neumann's boundary condition is prescribed on the anode and cathode for electron and ion densities. Electric potential is 0 V on the cathode and 25 000 V on the anode

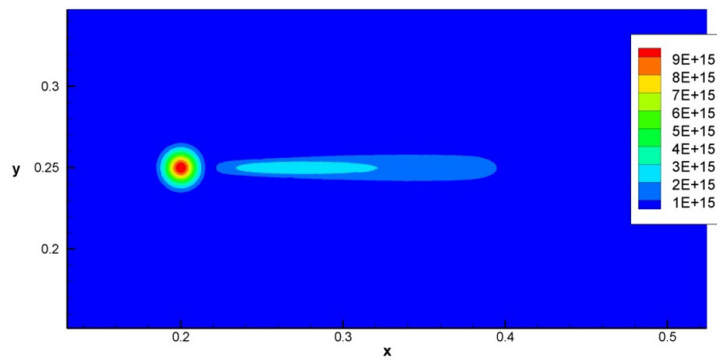
$$\begin{aligned} \frac{\partial \mathbf{n}_e}{\partial \vec{n}}(0, y, t) &= 0, \\ \frac{\partial \mathbf{n}_e}{\partial \vec{n}}(1, y, t) &= 0, \\ V(0, y, t) &= 25\,000 \text{ [V]}, \\ V(1, y, t) &= 0 \text{ [V]}. \end{aligned} \quad (16)$$

We used either Newton's homogeneous or periodical boundary condition for upper and lower boundary.

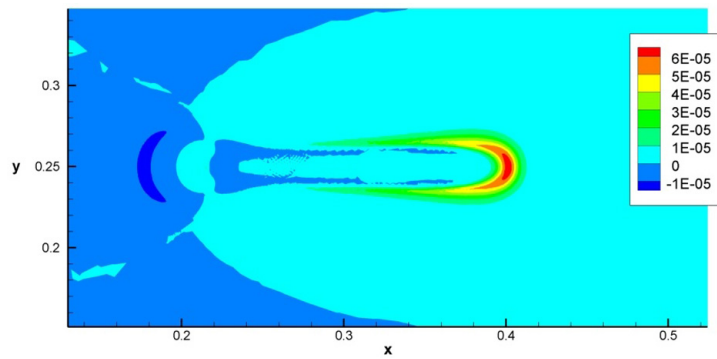
5. Results

A typical example of discharge motion is shown in Fig. 2. Electron density is plotted in Fig. 2a at time $t = 5.25 \cdot 10^{-8}$ s. We can see an initial pulse in position of $[x_0; y_0]$ and avalanche of electrons parallel with the x coordinate, discharge head is appropriately in the position $[0.4; 0.25]$ cm. We can observe charge with high magnitude — red color in Fig. 2b. This Figure shows isolines of the net-charge density

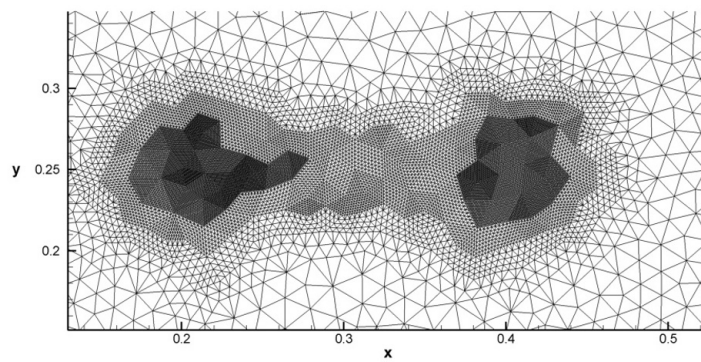
$$\rho = -\frac{e(\mathbf{n}_i - \mathbf{n}_e)}{\epsilon \cdot 10^4}, \quad (17)$$



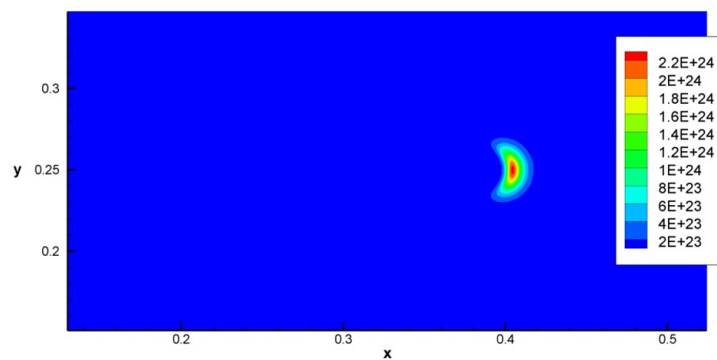
(a) Electron density



(b) Net-charge density



(c) Adapted grid



(d) Source term

Fig. 2. Results in time $t = 5.25 \cdot 10^{-8}$ s

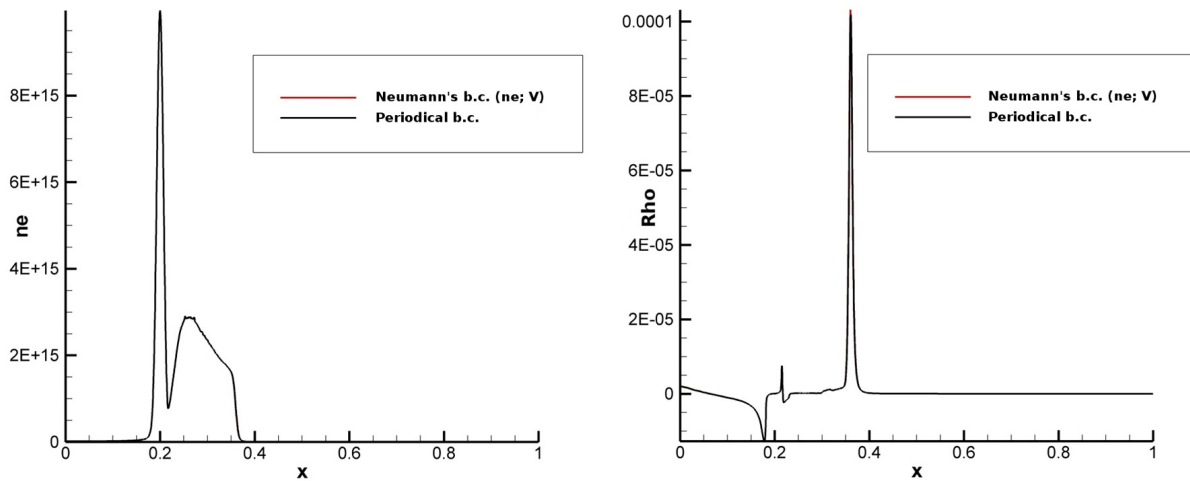


Fig. 3. Electron density (left), net-charge density (right) at time $t = 5.25 \cdot 10^{-8}$ s

corresponding to the right hand side of Poisson's equation (3). This relates to the narrow region with high values of source term (S_e) displayed in Fig. 2d. Therefore, we need grid refinement corresponding to the gradient n_e and magnitude of S_e . Our refined grid is plotted in Fig. 2c.

The comparison of the results of computations with Neumann's and periodical boundary conditions for the upper and the lower boundaries is shown in Fig. 3. There is electron density (left) and net-charge density (right) along line $y = 0.25$ cm. The figures confirm that results are almost identical and do not depend on type of boundary condition prescribed on the upper and lower boundary of the computational domain. Therefore, we use further only the Newton's boundary condition.

Figs. 4 and 5 illustrate dependence of the results on the width of the computational domain. Electron density computed by the first (left) and the second (right) order of accuracy along line $y = 0.25$ cm is shown in Fig. 4, net-charge density is in Fig. 5. These figures document increase of discharge head velocity with increasing width of the computational domain. Discharge head is shown (for electron density) as nearly vertical line which has the farthest position on the x coordinate, or in case of the net-charge density, as peek. Results computed on a domain with width 1.5 cm and higher are almost the same and we can take them as independent on the domain width.

The results of numerical convergence tests are shown in Figs. 6 and 7. We plot the electron density and the distribution of net-charge density along line $y = 0.25$ cm in the same time calculated on series of adapted grids with increasing maximal level of adaptation. We can observe the significant influence on grid density as well as much better convergence of second order approximation of convective term. Computation with the first order of accuracy shows decrease in velocity of discharge head with increasing number of adaptation levels. But computation with the second order of accuracy shows increase in velocity of discharge head with increasing number of adaptation levels. Solutions obtained from both orders of accuracy are moving towards each other. Results calculated by second order scheme are almost without differences for adaptation level 4 and higher. Therefore, we take 4th level of adaptation as satisfying compromise between accuracy and CPU time.

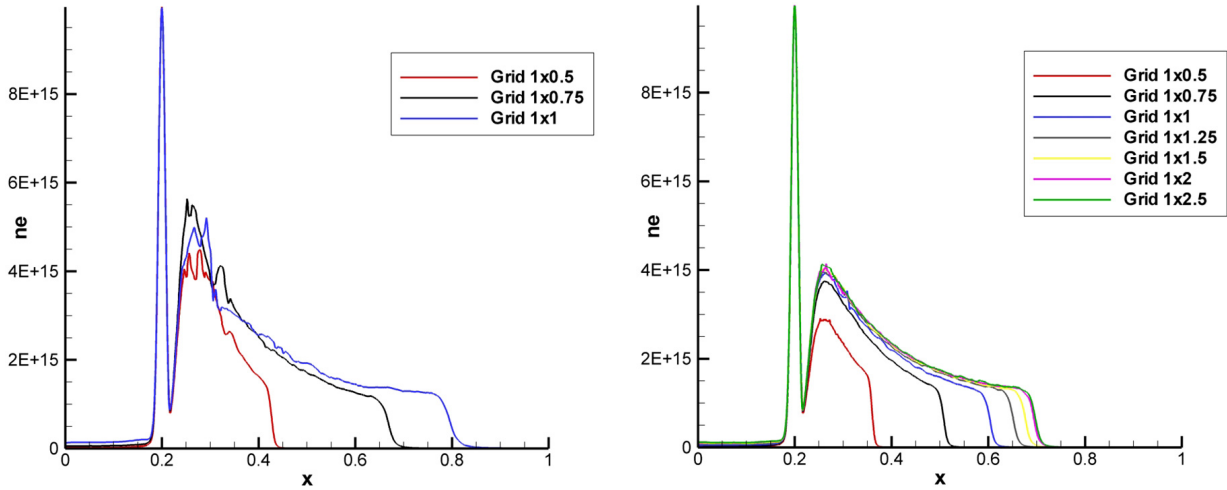


Fig. 4. Electron density at time $t = 5.25 \cdot 10^{-8}$ s and its dependence on domain width, 1st order (left) and 2nd order (right)

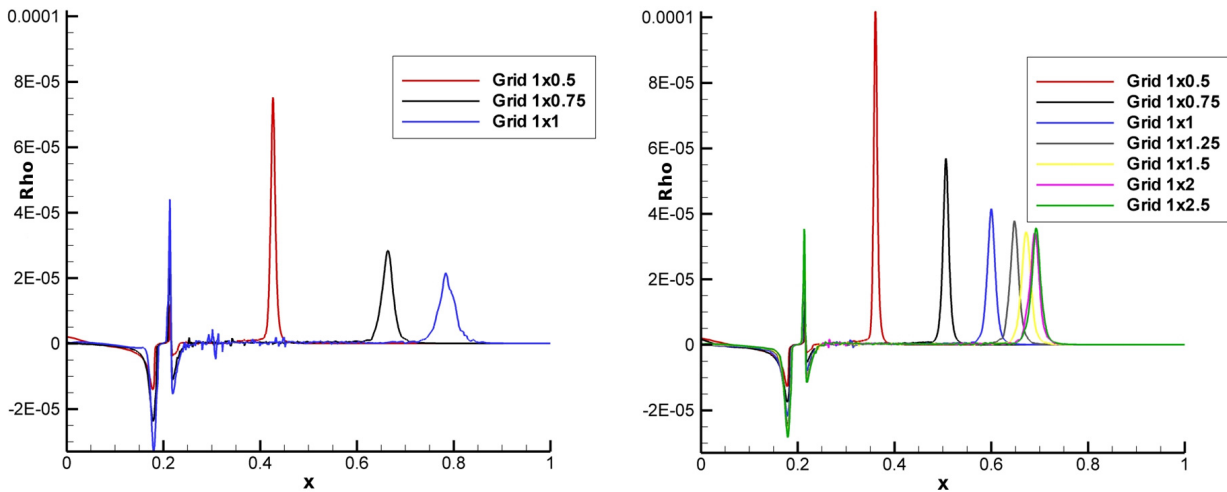


Fig. 5. Net-charge density at time $t = 5.25 \cdot 10^{-8}$ s and its dependence on domain width, 1st order (left) and 2nd order (right)

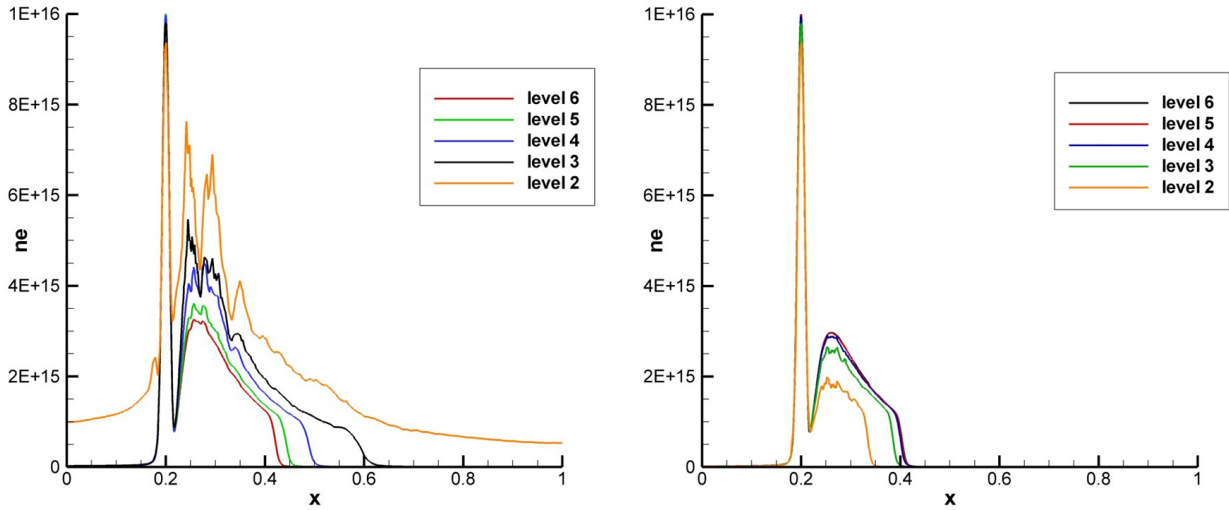


Fig. 6. Electron density at time $t = 5.25 \cdot 10^{-8}$ s and its dependence on refinement level, 1st order (left) and 2nd order (right)

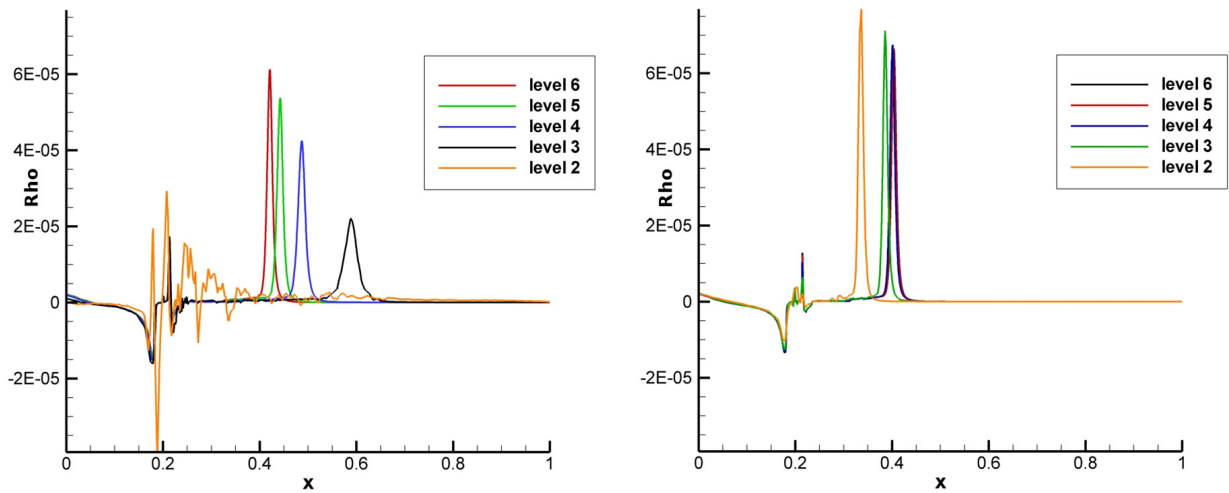


Fig. 7. Net-charge density at time $t = 5.25 \cdot 10^{-8}$ s and its dependence on refinement level, 1st order (left) and 2nd order (right)

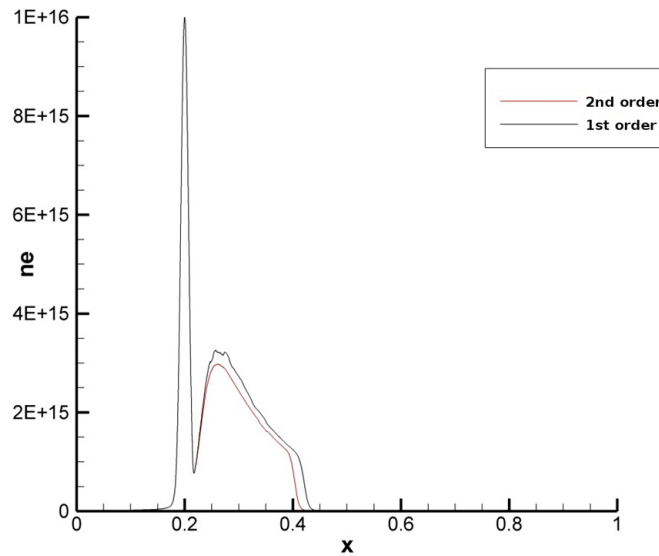


Fig. 8. Electron density for the 6th level of refinement, time $t = 5.25 \cdot 10^{-8}$ s, 1st and 2nd order

The proximity of the results for 6th level of refinement computed by 1st and 2nd order of accuracy illustrates Fig. 8. We can see only small difference in magnitude of the electron density and in the position of discharge head.

Table 1. The dependence of CPU time on adaptation levels

Level	Number of cells	Number of time steps	CPU time
2	5 024	2 395	0.009 9
3	10 592	10 607	0.089 6
4	41 082	24 552	1.000 0
5	62 392	56 629	3.840 0
6	186 802	153 090	31.800 0

Table 1 shows computational consumption in dependence on the maximal adaptation level. The table also contains numbers of cells and numbers of time steps for appropriate adaptation levels. Values of CPU time are scaled to the one with regard to the 4th level of adaptation, which is used as the reference value.

6. Conclusion

Presented results confirm ability of the numerical method and the grid adaptation strategy to capture the main features of planar discharge motion. They also show that for sufficiently wide (1.5 or 2 times distance of electrodes) computational domain can be prescribed relatively simple boundary conditions (homogenous Neumann or periodical condition) along artificial side boundaries without influence on the discharge propagation. Numerical convergence tests have been presented with conclusions that behavior of the first and the second order scheme differs with increased grid refinement level. Four levels of adaptation seems to be an optimal compromise between accuracy and efficiency of computation.

Acknowledgements

This work was supported by the Grant Agency of the Czech Technical University in Prague, grant No. SGS13/174/OHK2/3T/12.

References

- [1] Bartoš, P., Hrach, R., Jelínek, P., Multidimensional fluid-particle modelling technique in low-temperature argon plasma at low pressure, *Vacuum* 82 (2) (2007) 220–223.
- [2] Benkhaldoun, F., Fořt, J., Hassouni, K., Karel, J., Simulation of planar ionization wave front propagation on an unstructured adaptive grid, *Journal of Computational and Applied Mathematics* 236 (2012) 4 623–4 634.
- [3] Bourdon, A., Bessieres, D., Paillol, J., Michau, A., Hassouni, K., Marode, E., Ségur, P., Influence of numerical schemes on positive streamer propagation, *Proceedings of the 27th International Conference on Phenomena in Ionized Gases (ICPIG)*, Eindhoven, Netherlands, 2005, pp. 17 422.
- [4] Bourdon, A., Pasko, V. P., Liu, N. Y., Célestin, S., Ségur, P., Marode, E., Efficient models for photoionization produced by non-thermal gas discharges in air based on radiative transfer and the Helmholtz equations, *Plasma Sources Science and Technology* 16 (3) (2007) 656–678.
- [5] Montijn, C., Hundsdorfer, W., Ebert, U., An adaptive grid refinement strategy for the simulation of negative streamers, *Journal of Computational Physics* 219 (2) (2006) 801–835.
- [6] Morrow, R., Lowke, J. J., Streamer propagation in air, *Journal of Physics D: Applied Physics* 30 (4) (1997) 614–627.
- [7] Nikandrov, D. S., Arslanbekov, R. R., Kolobov, V. I., Streamer simulations with dynamically adaptive cartesian mesh, *IEEE Transactions on Plasma Science* 36 (4) (2008) 932–933.